Heterogeneous pores distribution in polyurethane expanding foams detected *via* X-ray computed microtomography

Aurelia Blazejczyk[1), *)], Paulina Wierzbicka[1)]

DOI: dx.doi.org/10.14314/polimery.2018.10.4

Abstract: X-ray computed microtomography (μ-CT) was applied as a noninvasive three-dimensional (3D) imaging technique for characterization of solid cellular material microstructure. Comparison between morphologies of two versions (summer and winter) of polyurethane (PUR) expanding foam (commercially available as the one-component 1K hand-held foams, applicable in building sector) was done. The evident relationship between processing and microstructure was explained. The most significant morphometric parameters were obtained *via* quantitative and qualitative 3D microstructure μ-CT analysis. The analysis embraced computing: dimensions of the selected structural elements (struts or pores), the average surface areas and volumes either of solid matrix or pores (open and close), as well as porosity assessment. The pores diameters (structure separation) statistical distributions were found and resulted as heterogeneous for both PUR versions, as revealed *via* proposed Gaussian μ-CT data analysis ("double Gauss" model).

Keywords: X-ray computed microtomography, foam imaging, polyurethane foams, pores, struts.

Niejednorodność rozkładu porów w ekspandujących piankach poliuretanowych obserwowana metodą mikrotomografii komputerowej

Streszczenie: Do charakterystyki mikrostruktury materiału komórkowego zastosowano rentgenowską mikrotomografię komputerową (μ-CT) – nieinwazyjną technikę obrazowania trójwymiarowego (3D). Porównano morfologie dwóch wersji (letniej i zimowej) pianki poliuretanowej (PUR), dostępnej w handlu w postaci jednoskładnikowej ekspandującej pianki typu 1K do zastosowań w budownictwie. Omówiono zaobserwowaną zależność między technologią przetwarzania a mikrostrukturą pianki. Na podstawie ilościowej i jakościowej mikrotomograficznej analizy trójwymiarowej mikrostruktury, obejmującej obliczenia wymiarów podstawowych elementów struktury (więzadeł i porów), a także powierzchni i objętości matrycy stałej i porów (otwartych i zamkniętych), wyznaczono najistotniejsze parametry morfometryczne. Dokonano też oceny porowatości pianki. Rozkłady średnic porów (*structure separation*) uzyskane w wyniku zaproponowanej gaussowskiej analizy danych mikrotomograficznych (*double Gauss model*) okazały się niejednorodne w wypadku obu wersji pianek PUR.

Słowa kluczowe: rentgenowska mikrotomografia komputerowa, obrazowanie pianki, pianki poliuretanowe, pory, więzadła.

The X-ray computed microtomography (μ-CT) is a standard tool for measuring and visualizing solid materials' microstructure. This measurement modality allows precise computing of numerous structural parameters, as well as imaging of the three-dimensional (3D) microstructures of specific materials, in particular porous cellular. These materials base on the solid matrix (polymer, ceramic, metal or carbon, *etc*.) forming walls, windows, struts or larger structural elements as cells.

For the open-celled polymeric foams, the term pore could be defined as a polygonal opening (interface window, eyelet) and the term strut as a ligament of the skeletal frame (forming the solid matrix network). In other words, the pore is an open (void) space embraced by a local polygon drawn by struts, while the strut is a local matrix node-node junction, where the node is the strut-strut intersection in the polygon vertex. The open-cell is formed by a "bubble" cluster of connected polygons. For the close-celled polymeric foams, the term pore could be defined as void space limited by adjacent polygonal

[1)] Warsaw University of Life Sciences – SGGW, Department of Civil Engineering, Faculty of Civil and Environmental Engineering, Nowoursynowska 159, 02-776 Warsaw, Poland.
[*)] Author for correspondence:
e-mail: pub.wbis.sggw@gmail.com

walls, forming a close-cell, and the strut is a common edge joining any two walls within the cell or wall-wall intersection. For the sake of simplicity, during the μ-CT analysis one may assume that pores and cells are the same 3D items. The term pore will refer to the combined void space of both cell and its interface windows, independently on the open- or close-cell foam's structure. In this context, the pore size can be estimated as the diameter of largest sphere inscribed (effectively fitted) into the limited pore space. Also, the term strut includes the nodes at its both ends. In this context, the strut size can be estimated as the diameter of largest sphere inscribed and limited by surface of the strut solid.

On one hand, the structural parameter used in macroscopic characterization of solid foams could be the relative density ϱ_r, defined as:

$$\varrho_r = \frac{\varrho}{\varrho_s} \tag{1}$$

where: ϱ – denotes the foam sample bulk (solid and gas state) density, ϱ_s – stands for density of the solid matrix [1]. On the other hand, the structural parameter describing microscopic scale could be the pores size. In general, size of a pore is the value based on its width, *i.e.*, base diameter of a cylindrical pore, distance between two sides of a slide-shaped pore, or the smallest dimension characterizing a fissure pore [2]. In the case of solid foams, pore size could practically be estimated by diameter of the largest sphere effectively inscribed within the pore; otherwise, pore size is an average diameter of the pore perpendicular cross-sections.

Based on the μ-CT analysis of the pores diameters distribution, one may assess if the material is homogeneously porous. Heterogeneously porous material would reveal more complex than just a single standard normal distribution.

The other important structural parameters are the number density of pores (per total number of structural objects detected), the total surface area of close or open pores and their volume for a solid foam sample. When characterizing the foam microstructure, one may additionally detect and recognize various topological states to reveal open pores, close pores, partially open pores, or mixed pores [1, 3]. The resulted foam 3D model covers the topology (close 3D geometrical relatives), dimensions and locations (coordinates) of the pores, struts or walls, which build the foam structure.

Pores in solid materials are classified as shown in Table 1 [4, 5]. Considering origin of pores formation, the term intra describes pores inside, while the term inter amongst the individual particles, cells, grains or crystallites. Considering their size (given by IUPAC), the pores can be micro- or meso- (of nanometric size) or macropores (of micrometric size) [6, 7]. Considering their topological state, the pores can be open or close. Considering their frame strength and thermal behavior, the pores can be rigid or flexible.

The intrinsic intra-particle pores may originate from defects in a material crystal structure (*e.g.*, of graphite), while the extrinsic intra-particle pores can be induced by doping foreign substances, *e.g.*, when the graphite carbon layers are expanded by intercalation with ions or more complex compounds [5, 8]. The inter-particle pores may be formed by space between molecules or chains (*e.g.*, in polymers). In the case of non-granular foams, the intra-cell pore is void space limited by walls within close-cell,

T a b l e 1. Existing classifications of pores in solid materials

1.	Based on the origin of formation:	
	Intra-particle pores	Intrinsic intra-particle pores Extrinsic intra-particle pores
	Inter-particle pores Intra-/inter-cell pores Intra-/inter-grain pores	(Proposed herein)
2.	Based on size (by IUPAC):	
	Micropores (< 2 nm)	Ultra-micropores (< 0.7 nm) Super-micropores (< 2.0 nm)
	Mesopores (2–50 nm)	
	Macropores (> 50 nm)	Sub-macropores (50–1000 nm) Real macropores (1–100 μm) Over capillary macropores (> 100 μm)
3.	Based on typological state:	
	Open pores/partially open	(Transitive)
	Mixed pores	(Dead ended)
	Close pores	(Latent)
4.	Based on pore frame strength:	
	Rigid	(Hard)
	Flexible	(Soft)

e.g., extruded polystyrene (XPS), while the inter-cell pore is void space limited by walls of neighboring foam cells or an intersection of two open cells (see also the Results and discussion). In the case of granular foams, the intra--grain pore could be inside a grain, *e.g.*, in expanded polystyrene (EPS) bead, while the inter-grain pore is the void space among grains, *e.g.*, among EPS beads [9, 10].

The real macropores (up to 100 μm) and the over capillary macropores (up to 1000 μm) could be detected, *e.g.*, in the tested PUR expanding foams by means of the μ-CT.

Based on pore state, the micropores form adsorption area for gas molecules, while the mesopores form the area of capillary condensation and allow for gas diffusion, and the macropores form the space for laminar fluid flow (gas or liquid) and most of all influence on lower bulk density. The open pores could be detected by GA (gas adsorption) method [6, 7]. Yet, if some pores were too small for the testing gas molecules, they could be detected by other methods, *e.g.*, SEM (scanning electron microscopy) or SAXS (small-angle X-ray scattering), which also can identify either open or close pores [5, 11].

Due to different pore frame strength, the hard pores are durable and the soft pores are easily deformable (*e.g.*, by temperature or external stress).

Since nanotechnology recently attracts the attention of scientists, such expressions as nanopores or nanoporous materials are often used despite the definition of nanopores is not yet established [5].

EXPERIMENTAL PART

Materials

The tested polyurethane PUR expanding foams are commercial products, manufactured by Soudal Sp. z o.o. in Poland (Soudal N.V. Belgium subsidiary).

The PUR expanding foams used to be applied in construction industry as fillings of cracks or voids in joinery, also, as sealing and noise nuisance in window sills, shutters, stairs, cable and pipe penetrations, as well as insulation in central heating, water-sanitation, plumbing and cooling systems, *etc*.

The tested material is commercially available in the two product versions: the "summer" (S) version and the "winter" (W) version (Soudal PU Mounting Foam). The latter is offered with special formula for application at low temperature, even at -10 °C.

The chemical composition and information of ingredients as propellant and blowing gases are given in Material Safety Data Sheet (MSDS) provided by manufacturer.

Preparing samples

The large steel casting mold was moisturized with water sprayed and filled by initial expanding mass of the commercial PUR product, which was left for free expansion at temperature 20 ± 1 °C and relative humidity 99 ± 1 % directly after moisturizing the casting mold. This allowed obtaining the rectangular hardened foam panels of dimensions 600 × 600 × 20 (width, length, height in mm) for both S- and W-versions. Average bulk density of the hardened foams resulted as 27 ± 2 kg/m^3 for both sample versions. The panels were later conditioned under controlled stable laboratory conditions at temperature 20 ± 1 °C and relative humidity 50 ± 5 % of environment for two weeks.

The rectangular prism form was formed, concerning planned thermal conductivity supplementary measurements (Fig. 1a). About half way from the center to edge of the PUR panel, the small cube was cut out the manner shown in Fig. 1a. Finally, the μ-CT sample was formed from the cube as 20 × 20 (diameter, height in mm) cylinder. Both S- and W-foam samples are shown in Fig. 1b. The cylindrical samples were formed from the small cubes so that their heights were along the *z*-axis or *q*-vector, perpendicular to the PUR expansion direction. Some microstructure anisotropy (in terms of cells expansion to-

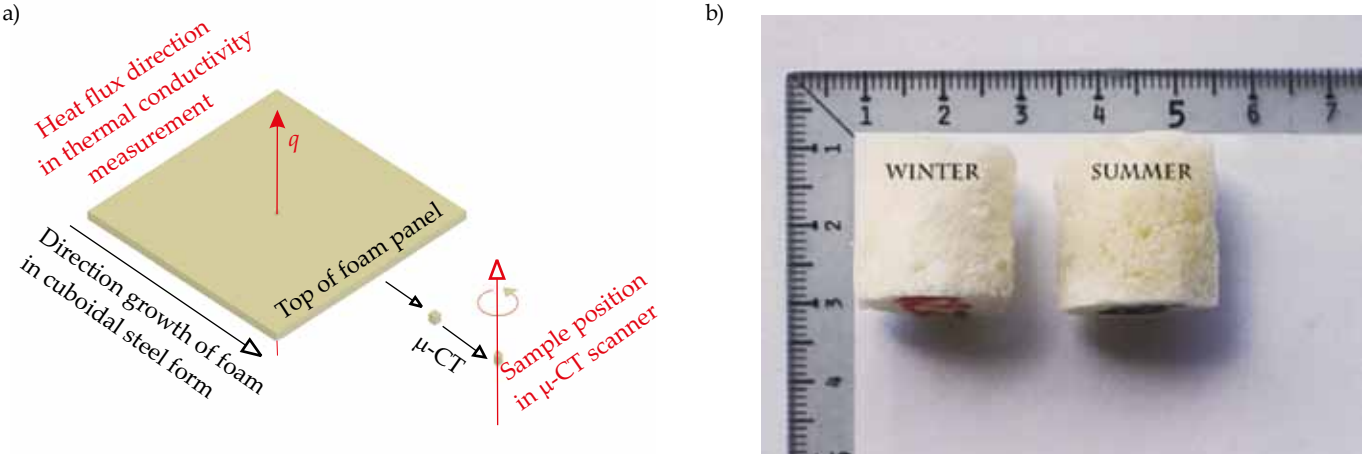

Fig. 1. a) Preparing samples from PUR foam – cutting a cuboidal sample along with foam growth direction *x* and forming cylindrical sample; the sample rotation is around the *z*-axis – parallel to vector *q* and perpendicular to the μ-CT scanner holder *xy*-plane, the sample to panel size ratio is kept the same as original, b) the enlarged W- and S-version samples are shown as placed on the *xz*-plane

wards *x*-axis) is then expected. This effect might cause directional dependence of thermal conduction in the hardened PUR foam panel.

Methods of testing

Scanning procedure

Scanning was done with the SkyScan 1172 μ-CT X-ray scanner (Bruker microCT). Some technical specifications of the scanner are given in Table 2.

The cylindrical samples prepared for μ-CT measurement were stacked one on the top of the other and fixed together with the base of the scanner sample holder by using special glue. It was positioned as shown in Fig. 1a – to ensure rotation around the axis perpendicular to the sample holder plane.

Detailed description of the scan settings and their effect on image quality has been described elsewhere [12–15], however, only some optimal parameters for the μ-CT scanning (Table 3) have been selected in this case.

The μ-CT scans for both S- and W-versions of the PUR foam were obtained in the cone X-ray beam acquisition. The acquired dataset consists of 2925 rotation image 2D vertical-projections (scans) in 16-bit TIFF format (4000 × 2664 pixels) for the two samples stack. The scanning process took about 180 minutes and was carried out at constant temperature.

T a b l e 2. Technical specifications of the SkyScan 1172 μ-CT X-ray scanner

X-ray source	X-ray lamp (Hamamatsu L7902-20)
X-ray detector	X-ray SHT 11Mp CCD camera (Ximea MH110XC-KK-FA)
Image pixel range, μm	1–25

T a b l e 3. The microtomography settings

	Material version	
	S-foam	W-foam
Physical dimensions of the cylindrical samples (diameter; height), mm	20; 20	20; 20
Flat field correction	Activated	Activated
Median filtering	Activated	Activated
Geometrical correction	Activated	Activated
External filter on detector	Not activated	Not activated
X-ray source voltage, kV	33	33
X-ray source current, μA	204	204
Number of rows on camera matrix	2664	2664
Number of columns on camera matrix	4000	4000
X-ray detector binning	1 × 1	1 × 1
Number of connected scans per step (oversized scanning mode)	3	3
Rotation sections count (total number of scans)	2925	2925
Exposure time, ms	1680	1680
Rotation range, deg	0–195	0–195
Rotational step, deg	0.2	0.2
Random movement amplitude (number of lines on camera matrix)	40	40
Frame averaging (number of frames averaged in each step)	4	4
Image pixel size, μm	6.25	6.25

Choice of the region and volume of interest and image reconstruction

For each sample the 3D cross-sectional image stack was reconstructed from the rotation image 2D vertical-projections, by using the NRecon cone X-ray beam reconstruction software (Bruker microCT), based on the Feldkamp algorithm. The NRecon software allowed us adjusting four of the reconstruction parameters: smoothing, post-alignment, ring artefact reduction and beam-hardening factor correction. All of the parameters had to be found experimentally *via* the try & error method, also basing on literature [16]. The resulted optimal settings are listed in Table 4.

Before reconstruction, the appropriate region of interest (ROI) was defined, together with its reduced size

T a b l e 4. The microtomography parameters used in image reconstruction of the PUR foams

Parameter, unit	Material version	
	S-foam	W-foam
Dimensions of 3D cross-sectional image stack (width; length; height), mm	22.3; 22.3; 11.1	22.3; 22.3; 11.1
Sections (images) count	1771	1771
First section (image number without glue layer)	3650	330
Last section (image number about sample mid-height)	5420	2100
Reconstruction from region of interest (ROI)	Activated	Activated
ROI reference length (side of square), pixel	3572	3572
Resulted image size, pixel	3572 × 3572	3572 × 3572
Reconstruction angular range, deg	0–180	0–180
Smoothing	0	0
Misalignment compensation (post-alignment)	-2.0	-2.0
Ring artefact reduction	1	1
Beam hardening correction, %	10	10
Image pixel size, μm	6.25	6.25

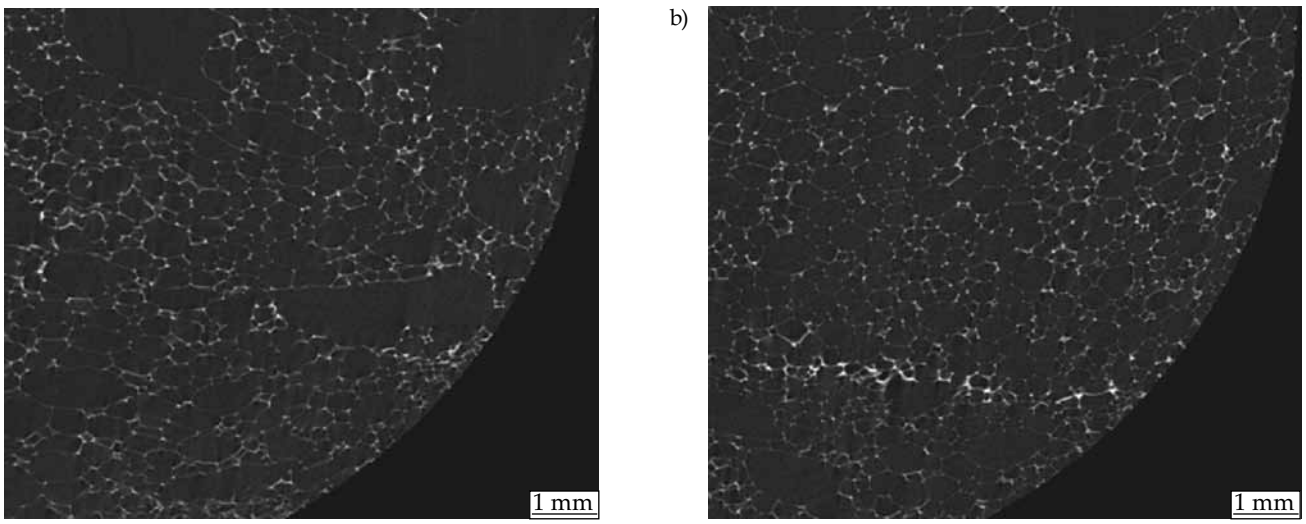

Fig. 2. 2D cross-sectional images (quarters) of the reconstructed 3D image stack, representing W-version of the PUR foam, after reselection of circular ROI and 4× resized; the white pixels in ROI represent the PUR foam struts, while the dark grey pixels represent void space: a) first section 0083 (corresponding to 330) – the horizontal xy plane, b) last section 0525 (corresponding to 2100) – the horizontal xy plane

(from default 4000 × 4000 down to 3572 × 3572 pixels squared) and shape and location in each single 2D cross-sectional image (cross-section), in previous mode. The reconstruction was performed within the volume of interest (VOI), which refers to a sum of a number of ROIs over a set of 2D cross-sectional images. The VOI is a 3D space integrated from the stacked images. When defining VOI size (by setting a number of cross-sections for each sample), uneven distribution of the PUR foam structure was carefully considered. Additionally, all glue layers images were removed (by setting a position of first section for each sample) before 3D image reconstruction – to avoid affecting the μ-CT structural analysis of the foam samples. Hence, dataset resulted from reconstruction consisted of 1771 8-bit BMP images per each sample. As a result, for both S- and W-version of the PUR foam, the selected 3D volume corresponds to approximately half of the sample volume.

The 16-bit TIFF format, despite containing more information than 8-bit BMP, does not provide saving of color palette and allows to represent objects in grey scale only. Colors may have importance for further detailed image analysis and visualization.

Input parameters and image analysis

After reconstruction (carried out for each sample independently by NRecon), the 3D cross-sectional image stacks were further processed by CTAn software (Bruker microCT) [17].

During the 3D image analysis, firstly, the ROI regions were reselected by changing their shape (from square to circle) and reducing their size (from 22.3 to 18 mm) – to cut off apparent border effects. Examples of the 2D cross-sectional images (as only quarters) within the ROIs are presented in Fig. 2 for W-foam sample.

The terminal size of the 3D cross-sectional image stack was set as 4 times resampled (443 images) than the default size (1771 images from reconstruction). This resulted in the 4 times resized pixel size (4× resized). Such action was car-

T a b l e 5. The microtomography input parameters used in analysis of the PUR foams

Input parameter, unit	Material version	
	S-foam	W-foam
Dimensions of 3D cross-sectional image stack (diameter; height), mm	18; 11.1	18; 11.1
Sections count	443	443
First section	913	83
Last section	1355	525
Reconstruction from region of interest (ROI)	Activated	Activated
ROI reference length (circle diameter), pixel	720	720
Resulted image (square) size, pixel	724 × 724	724 × 724
Image pixel size, μm	25.01	25.01
CTAn analysis settings		
Thresholding (global mode): – lower grey threshold (fixed manually) – upper grey threshold	 41 255	 41 255
Despeckle (white-speckle mode in 3D space): – remove white dots smaller than, voxels	 1	 1
ROI shrink-wrap (shrink-wrap mode in 2D space): – stretch over blow holes of a diameter above, pixels	 20	 18
Save bitmaps (image inside ROI mode)	Activated	Activated
3D analysis	Activated	Activated

T a b l e 6. The morphometric output parameters describing the PUR foams

Output parameter, unit	Abbreviation	Material version	
		S-foam	W-foam
Dimensions of 3D cross-sectional image stack (diameter; height), mm		18; 11.1	18; 11.1
Total VOI volume, mm^3	TV	2844	2844
Object volume (matrix only), mm^3	Obj.V	384	436
Volume of close pores, mm^3	Po.V(cl)	0.2	0.3
Volume of open pore space, mm^3	Po.V(op)	2459.8	2407.5
Total volume of pore space, mm^3	Po.V(tot)	2460.0	2407.9
Total VOI surface, mm^2	TS	1177	1177
Object surface (matrix), mm^2	Obj.S	30 225	34 031
Surface of close pores, mm^2	Po.S(cl)	40	64
Number of objects (detected)	Obj.N	323 348	128 963
Number of close pores	Po.N(cl)	7233	12 063
Percent object volume, %	Obj.V/TV	13.5	15.3
Close porosity, %	Po(cl)	0.05	0.08
Open porosity, %	Po(op)	86.5	84.7
Total porosity, %	Po(tot)	86.5	84.7
Structure separation (pore diameters) average value, mm	St.Sp	0.413	0.317
Structure thickness (strut diameters) average value, mm	St.Th	0.051	0.052

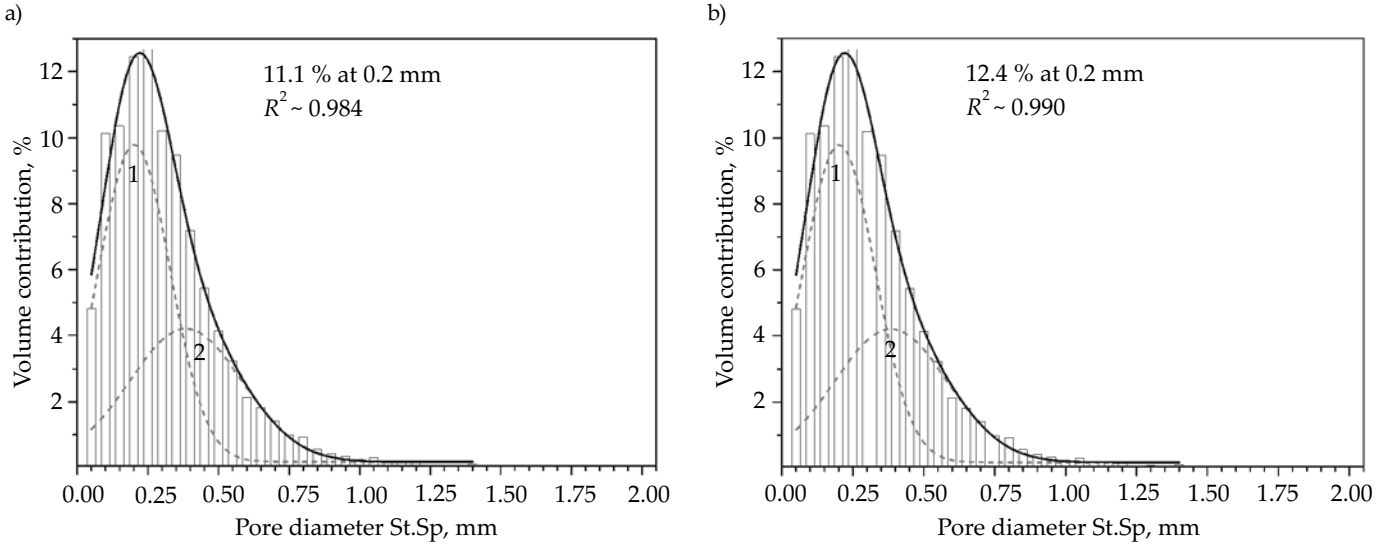

Fitted peaks parameters, mm:

	Center	Width	Height
1.	0.18	0.22	7.5
2.	0.37	0.45	4.7

Fitted peaks parameters, mm:

	Center	Width	Height
1.	0.20	0.25	9.6
2.	0.38	0.40	4.0

Fig. 3. Apparent distributions of the pores diameters (structure separation) for PUR foams (4× resized) – bar graphs: a) S-foam, b) W-foam; the thick solid lines represent the sum of the two overlapped peak-components, the dashed lines represent the separated distributions by Gaussian analysis (discussed in later text); the explicit maxima of the total (effective) fitted distributions (solid lines): 11.1 % (S) and 12.4 % (W) at 0.2 mm, can be compared with structure separation parameters from Table 6

ried out in order to speed up visualization of the structure by using the 3D visualization software. For the sake of simplicity, the 4 times resampled data set VOI was preserved for each sample, since it allows finding the main morphometric parameters necessary to characterize the tested PUR foam structures and clarify the observed effects.

In CTAn the following settings were additionally adjusted: thresholding, removing speckles, and ROI shrink-wrap. After the ROI reselection, the 2D cross-sectional images were binarized by manually selected a lower grey-level threshold, above which voxels were considered as material and below which as background. The tresholding (segmentation) was done on a histogram from the dataset for both entire 3D cross-sectional image stacks by simple global method.

The optimal values (optimized for each foam sample) of input parameters used in 3D image analysis are shown in Table 5.

In the course of the activated analysis, the parameters describing the PUR foam structure were computed together with 3D model building, based on the binarized 3D image voxels distribution.

RESULTS AND DISCUSSION

Output parameters

After analysis by CTAn software, some of the possible output parameters [18] were selected and listed in Table 6.

The following expressions explain the relations between the parameters listed in Table 6:

$$TV = Obj.V + Po.V(cl) + Po.V(op) \quad (2)$$

$$Po.V(tot) = Po.V(cl) + Po.V(op) = TV - Obj.V \quad (3)$$

$$Po(cl) = Po.V(cl)/Obj.V \cdot 100\ \% \quad (4)$$

$$Po(op) = Po.V(op)/TV \cdot 100\ \% \quad (5)$$

$$Po(tot) = [Po.V(op) + Po.V(cl)]/TV \cdot 100\ \% \quad (6)$$

One may note that both open porosity Po(op) and total porosity Po(tot) are expressed as a percentage of total volume TV, yet, the close porosity Po(cl) is expressed as a percentage of matrix volume Obj.V (in fact, it is a contribution to the matrix that forms the close pores, rather than to total void space in the sample).

As seen from Table 6, the percentage volume of the PUR matrix contribution in total volume of samples is higher for version W. Therefore, for this type of the commercial PUR foams, one may notice that the more percentage content of matrix the more percentage content of the close pores and the more surface of the close pores in matrix.

The Obj.S (total area of matrix in VOI) to TS (total area of cylindrical VOI space) ratio resulted nearly 30. That is understandable referring to complex structure of the solid matrix, which is tightly and densely packed in the 3D space of the VOI.

Total porosity resulted approximately 2 % higher for S- than for W-version of the PUR foam. The same percentage trend is evident for open porosity, although close porosity resulted slightly higher by approximately 0.03 % for the W-version.

Based on the CTAn output data, beside the morphometric parameters, distributions of the pores diameters for both S- and W-version of the PUR foam could be generated additionally. The apparent distributions in form of the bar graphs are shown in Fig. 3 – to be discussed later.

The structure visualization

The μ-CT analysis for both S- and W-version of the PUR foam could be completed by using CTvoxel software (Bruker microCT) [19].

The CTAn output of each sample (3D cross-sectional image stack) was transformed (by means of the built-in transfer function) into the realistic 3D visualization. It includes details of the PUR foam structure, which comprises the skeletal frame (forming the solid matrix net-

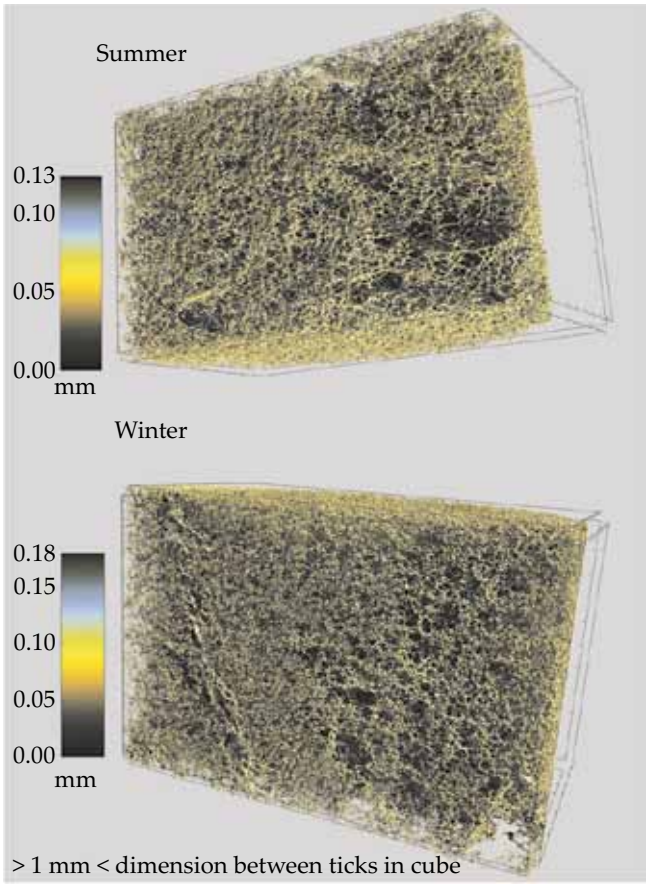

Fig. 4. The S- and W-foams 3D realistic visualization (4× resized) to show the solid matrix network; the cuboid base is in the horizontal *xy*-plane, the front wall is in the vertical *xz*-plane; the PUR expanding gases escaped through *yz*-plane on the right side, the left scale corresponds to the strut size (structure thickness)

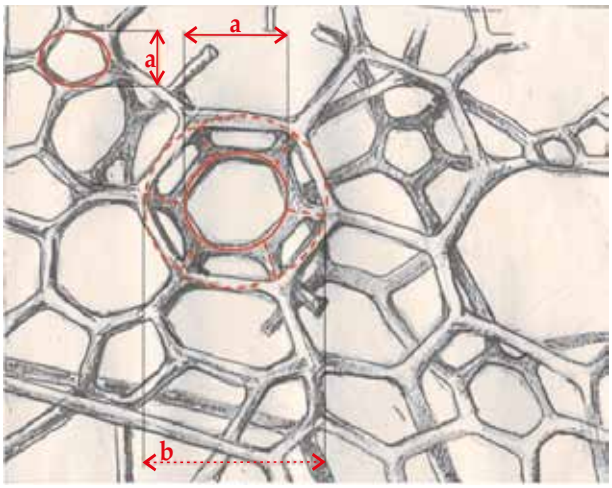

Fig. 5. The simplified sketch to distinguish between the pore as interface window [eyelet – (a)] and the pore as cell ["bubble" polygon cluster – (b)] in the open-cell PUR foams; the sketch corresponds to a part of the W-foam sample, shown in Fig. 4, seen from above the horizontal *xy*-plane

work) together with the pores and cells (forming the open channels network). In Fig. 4, matrix networks are shown for the corresponding S- and W-sample regions.

The simplified sketch shown in Fig. 5 was created to show porous microstructure and help explain difference between the window pore (eyelet) and the pore in cell ("bubble" polygon cluster) in the open-cell foams. This sketch is based on real 3D visualization of the tested W-foam sample, shown in Fig. 4, seen from above the horizontal *xy*-plane.

Discussion

Two series of individual bars (for S- and W-version of the PUR foam) in Fig. 3 correspond to the distributions of pores diameters in material. As seen from the apparent distributions and the computed average pore diameters (structure separation parameters in Table 6), the S-foam material is dominated by slightly larger pores of average diameter 0.4 mm, while the W-foam material is dominated by somewhat smaller 0.3 mm pores.

As expected, pore size depends on specific local microstructure, which might slightly vary through whole sample volume, so the pore population could be governed by a statistical distribution with a certain expected value (a mean pore diameter). The distribution spread depends on random fluctuations of the local environments around the pores. Since the most natural distribution in the case of such random fluctuations would be the standard normal distribution, one may assume that it properly reflects heterogeneity in pore size.

Interestingly, as seen from Fig. 3, the apparent distributions for both versions S- and W-foam show a visible asymmetry, since the right side is wider. To account for this effect, we proposed and succeed to fit the "double Gauss" model to the apparent distribution, within the whole range (from 0 to about 2 mm). The computed resultant sum of the two component Gaussian distributions (1 and 2) seems to provide a good envelope for the whole bar graph. Thus, the "double Gauss" model can be used to analyze the apparent distributions for both versions of the foams under study.

Comparing the two samples, one may notice that the fitted pores distribution for S-foam (solid line) reveals significantly wider spread than the W-foam. Also, the two separated components of the pore distribution for S-foam (dashed lines) reveal shift towards larger diameters. Moreover, the S-foam structure reveals existing pores of diameters above 1 mm, yet their distribution is significantly scattered and contribution negligibly low. Therefore, the latter third distribution component could not be taken into account in the course of data fitting and model finding procedure.

Based on the μ-CT analysis of the pore distribution, one may state that the material under study is not homogeneously porous. It reveals more complex distribution than just a single standard Gaussian, so both foams under study may be considered as heterogeneously porous. In other words, each foam structure might include minimum two coexisting types of 3D microstructures, formed by two different types of macro-pores of the detected diameter distributions. The smaller and larger pore diameters resulted of about 200 μm and 400 μm, respectively (Fig. 3). The presented cell windows in Fig. 5 indicate on at least two 2D geometrical shapes (penta- and hexagonal), from which the cells might be probably composed.

Processing-to-structure relationship found in the PUR expanding foams could be described by the apparent difference between the two S- and W-versions, shown in terms of the position and spread of the resulting pores distributions. The effect of processing on structure could be explained by understanding the impact of the interior and exterior environments on the expanding pores during foam formation. Besides solidifying matrix, the environment is the propellant and blowing gases used in processing. One of the recognized so far difference between the two S- and W-versions during foaming process is the presence of the 1,1-difluoroethane $C_2H_4F_2$ gas. This in particular might affect the foam structure morphology and thus size and 3D polyhedral form of the pores.

CONCLUSIONS

The X-ray μ-CT investigation of the PUR expanding foams allowed to classify the detected pores as inter-cell macro-pores (*i.e.*, real above 50 μm and over capillary macropores up to *ca.* 1000 μm), which are formed as a common intersection between neighboring open-cells of the material under study.

Firstly, the μ-CT analysis of the pore size distributions allowed assessing such structural property as homogeneity of PUR foams in terms of porosity that resulted heterogeneous. Secondly, when visualizing the foam structure, at least two different window shapes, which may

describe rather open than close pores, could be observed. Therefore, one may conclude that the PUR foam could be composed from the cells of at least two different geometrical 3D forms (defining pores) – based on assumption that the "single Gauss" component is related to distribution of polydispersed cells of unique topology (or close topological relatives). In order to fully characterize morphology of the foams, further study is required, in particular based on scanning electron microscope (SEM) measurement and a 3D structural model fitting.

Only macropores could be detected by means of the used method herein, the X-ray μ-CT. The order of magnitude of their diameters was about 100 μm, five orders of magnitude larger than the micropores (as defined by IUPAC). Nevertheless, still the μ-CT image processing offered a powerful tool that could be used to compute local 3D structure of materials.

The morphometric analysis, as well as 3D realistic visualization of both PUR foam versions, resulted in computed values – *ca*. 85 % for open porosity in overall VOI and less than 1 % for close porosity in PUR solid matrix, so the foam appeared to be predominantly open-cell material.

Since our research protocol provided accurate assessment of the 3D structure and valuable information about morphometric parameters of the PUR expanding foams, one may conclude that – whenever measuring the open- and close-cell foam materials (in order to quantify the volume fraction of open and close pores) – the μ-CT studies should become the first choice standard method, complementary to other techniques: SEM, gas pycnometry, SAXS, applied either by researchers or manufacturers.

The research was supported by: Comef Scientific & Research Equipment Company (Poland); Bruker microCT N.V. Company (Belgium); Poznan Supercomputing and Networking Center with PLATON – Service Platform for e-Science (Poland); Polish Culture, Art and Science Foundation "ALTERNATIVES" (Poland).

REFERENCES

[1] Salvo L., Martin G., Suard M. *et al*.: *Comptes Rendus Physique* **2014**, *15* (*8–9*), 662. http://dx.doi.org/10.1016/j.crhy.2014.10.006

[2] Zdravkov B.D., Čermák J.J., Šefara M., Janků J.: *Open Chemistry* **2007**, *5* (*2*), 358. http://dx.doi.org/10.2478/s11532-007-0017-9

[3] Gibson L.J., Ashby M.F.: "Cellular Solids: Structure and Properties 2nd ed.", Cambridge University Press 1997.

[4] Patrick J.W.: "Porosity in Carbons: Characterization and Applications 1st ed." Published by Edward Arnold, London 1995.

[5] Inagaki M.: *New Carbon Materials* **2009**, *24* (*3*), 193. http://dx.doi.org/10.1016/S1872-5805(08)60048-7

[6] Rouquerol J., Avnir D., Fairbridge C.W. *et al.: Pure and Applied Chemistry* **1994**, *66* (*8*), 1739. http://dx.doi.org/10.1351/pac199466081739

[7] a) Sing K.S.W.: *Pure and Applied Chemistry* **1985**, *57* (*4*), 603. http://dx.doi.org/10.1351/pac198557040603
b) IUPAC, "Compendium of Chemical Terminology 2nd ed." (The "Gold Book"). http://dx.doi.org/10.1351/goldbook

[8] Porada S., Zhao R., van der Wal A. *et al*.: *Progress in Materials Science* **2013**, *58* (*8*), 1388. http://dx.doi.org/10.1016/j.pmatsci.2013.03.005

[9] Coquard R., Baillis D., Quenard D.: *Journal of Heat Transfer* **2009**, *131* (*1*), 012702. http://dx.doi.org/10.1115/1.2994764

[10] Baillis D., Coquard R., Harifidy Randrianalisoa J. *et al*.: *Special Topics & Reviews in Porous Media: An International Journal* **2013**, *4* (*2*), 111. http://dx.doi.org/10.1615/SpecialTopicsRevPorousMedia.v4.i2.20

[11] Nishikawa K.: "Pore structure analyses of carbons by small-angle X-ray scattering" (Eds. Yasuda E., Inagaki M. *et al*.), Carbon Alloys, Elsevier, Amsterdam 2003, pp. 175–188.

[12] Montminy M.D., Tannenbaum A.R., Macosko C.W.: *Journal of Colloid and Interface Science* **2004**, *280* (*1*), 202. http://dx.doi.org/10.1016/j.jcis.2004.07.032

[13] Mader K., Mokso R., Raufaste C. *et al*.: *Colloids and Surfaces A: Physicochemical and Engineering Aspects* **2012**, *415*, 230. http://dx.doi.org/10.1016/j.colsurfa.2012.09.007

[14] Leszczyński B., Wróbel A., Gancarczyk A. *et al*.: "Morfology of carbon foams", Abstract Book, Micro-CT User Meeting 2014.

[15] Moesen M., Verniers K., Brennan M., Vandenbroeck J.: "Morfological analysis of polyurethane foams", Abstract Book, Micro-CT User Meeting 2015.

[16] Bruker microCT, SkyScan NRecon User Guide 2010.

[17] Bruker microCT, Manual for Bruker-microCT CT-Analyser version 1.13, User Guide.

[18] Bruker microCT, Morphometric parameters measured by Skyscan™ CT-analyser software, User Guide.

[19] Bruker microCT, CTvox Quick Start Guide for software version 2.4.

Received 24 I 2018.